Applied Clay Science 237 (2023) 106900

Contents lists available at ScienceDirect

Applied Clay Science

journal homepage: www.elsevier.com/locate/clay

Research Paper

Metakaolin-based geopolymer – Zeolite NaA composites as CO_2 adsorbents

Elettra Papa [a], Matteo Minelli [b], Maria Chiara Marchioni [a,c], Elena Landi [a], Francesco Miccio [a], Annalisa Natali Murri [a], Patricia Benito [a,c], Angelo Vaccari [a,c], Valentina Medri [a,*]

[a] National Research Council of Italy, Institute of Science, Technology and Sustainability for Ceramics (CNR-ISSMC former CNR-ISTEC), Via Granarolo 64, 48018 Faenza, RA, Italy

[b] Department of Civil, Chemical, Environmental and Materials Engineering (DICAM), Alma Mater Studiorum – University of Bologna, via Terracini 28, 40131 Bologna, Italy

[c] Dipartimento di Chimica Industriale "Toso Montanari", Alma Mater Studiorum – University of Bologna, Viale Risorgimento 4, 40136 Bologna, Italy

ARTICLE INFO

Keywords:
Geopolymer
Metakaolin
Composites
Zeolite nucleation
CO_2 adsorption

ABSTRACT

In this work, three metakaolin-based geopolymer matrices were prepared, varying the molar ratio Si:Al (2.0 or 1.2) and the type of cation (sodium or potassium). Starting from these matrices, geopolymer-zeolite composites were synthesized and consolidated (80 °C), incorporating a commercial sodium-based zeolite, Na4A, with the aim of producing post combustion CO_2 adsorbents, since the presence of Na4A crystalline phase is desirable due to its known remarkable CO_2 adsorption capacity.

The sodium-based geopolymer matrix with Si:Al = 1.2 allowed the *in situ* nucleation of the zeolite NaA, therefore this matrix was added with different amount of synthetic zeolite Na4A to verify the total conversion of the matrix into zeolite NaA, in view of an alternative low-cost synthesis method to obtain zeolite NaA as a "solid" in a complex form.

The composites were deeply characterized and lastly tested for CO_2 adsorption. The geopolymer matrices act as binders allowing the shaping of zeolite and producing functional composites with mutable chemical composition, microstructure and porosity according to the starting composition. The sodium-based geopolymer zeolite composite was the best performing in term of CO_2 adsorption capacity being 1.0 mmol g^{-1} at 0.1 bar, nearly equivalent to synthetic zeolite Na4A (1.2 mmol g^{-1}) and close to pure zeolite Na13X (1.4 mmol g^{-1}), the current benchmark material for carbon capture application.

1. Introduction

Davidovits coined the term geopolymer in the late 1970s, indicating materials of mineral/inorganic origin obtained by polycondensation that leads to an amorphous three-dimensional aluminosilicate network (Davidovits, 1991). Geopolymers are obtained by alkaline activation of an aluminosilicate precursor, which, because of polycondensation reactions at low temperature (generally below 100 °C), gives rise to the matrix. Such mechanism is named geopolymerization. The structure obtained is characterized by a connection of silicon and aluminum tetrahedras, which combined give origin to interconnected channels, rings and cages similar to that of zeolites (Breck, 1974; Rożek et al., 2019), although on different long-range order (Duxson et al., 2005). Not surprisingly, as reported by Kriven et al., 2003, geopolymers can be considered as "amorphous zeolites that have not had the opportunity to crystallize". Geopolymers are inherently porous materials, similarly to zeolites; in particular, they are mesoporous materials while zeolites are microporous. However, unlike zeolites, they have good mechanical properties and they are easily shaped (Landi et al., 2013). These characteristics make geopolymers very appealing either for structural use, as thermal and acoustic insulators, or as supports for catalysts (Cong and Cheng, 2021; Zhang et al., 2021). Furthermore, the synthesis of geopolymers is simpler and less energy-intensive than that of zeolites. Geopolymers can boast high mechanical performance with an easy shaping and reproducibility even on a large scale.

The characteristics of geopolymer materials strongly depend on the raw materials used, which have to be carefully selected for the desired application. For the synthesis of a geopolymer, three different types of raw materials are needed: aluminosilicate powder, alkaline activator and fillers. The selection of the aluminosilicate source, as a matter of

* Corresponding author at: National Research Council of Italy, Institute of Science, Technology and Sustainability for Ceramics (CNR-ISSMC former CNR-ISTEC), Via Granarolo 64, 48018 Faenza, RA, Italy.

E-mail addresses: valentina.medri@istec.cnr.it, valentina.medri@issmc.cnr.it (V. Medri).

https://doi.org/10.1016/j.clay.2023.106900
Received 24 November 2022; Received in revised form 2 February 2023; Accepted 5 March 2023
Available online 11 March 2023

fact, determines the Si:Al ratio, and therefore it controls the two or three-dimensional structure of the resulting geopolymer. That leads to different characteristics of the product (compressive strength, possibility of formation of crystalline phases, *etc.*) and its possible applications (Davidovits, 2008). Beside the use of waste raw materials such as fly ashes or slugs (Ren et al., 2021), the purest and most reactive is metakaolin deriving from thermal dihydroxylation of kaolin (Medri et al., 2010; Romero and Nishant, 2022).

The type of activator (generally solutions of alkali metal hydroxides and/or silicates) is selected based on the reactivity of the precursor powders and the type of cation to be introduced (usually sodium or potassium). The hydrolysis rate of the aluminosilicate powder, the rate of polycondensation and, consequently, the mechanical properties of the final material depend on the nature of the cation (Medri et al., 2010).

Finally, fillers, additives and/or pore-forming agents are added in order to impart specific properties or functionalities to the geopolymer material (rheological properties, dimensional stability, adequate porosity, new functions). In geopolymer-zeolite composites, for example, the peculiarities of the zeolites, used as fillers, are combined with those of the geopolymers (Rożek et al., 2019). In that way, the microporosity, the high surface area and the reactivity of the zeolites are combined with the mesoporosity, mechanical resistance and support provided by the geopolymer matrix (Papa et al., 2018; Rożek et al., 2019). Indeed, self-supporting, scale designable, porous and easy-to-handle materials, can be produced, allowing to consolidate effectively the zeolite phase, that is of great importance at the industrial level. That allows to obtain customized materials, potentially suitable in the most disparate fields. In fact, zeolites by virtue of their three-dimensional network can be classified as tecto-aluminosilicates with cation exchange properties. For this reason, zeolites are often used industrially for water softening, while the microporosity that characterizes them determines their use as catalysts, adsorbent materials, molecular sieves and materials used for the treatment of polluted water (Khaleque et al., 2020).

Geopolymer-zeolite composite materials can thus be used as solid adsorbents for the separation or the purification of aqueous or gaseous systems. Indeed, they are suitable for the purification of aqueous media, and in particular for large-scale wastewater treatment (Liu et al., 2016) or as bulk adsorbents of heavy metals (Lee et al., 2016). Furthermore, self-supported membranes can be produced exploiting the formation of a layer of zeolite on the geopolymer matrix used as support, increasing the mechanical resistance of the membrane (Xu et al., 2017). Geopolymer-zeolite composites find applications also in the building sector, since they have humidity control (Takeda et al., 2013) and thermo-insulating properties related to the release of the zeolite water during heating (Rożek et al., 2019).

Regarding the purification of gaseous systems, these materials are suitable to remove specific components, for instance in drying applications in air conditioning system (Wu et al., 2018), or as purifiers against toxic substances, such as formaldehyde (Huang et al., 2012), or as solid adsorbents for carbon dioxide (CO_2) removal (Papa et al., 2018; Minelli et al., 2018). Referring to this last example, it is noteworthy the synergistic effect found between the geopolymer matrix and the zeolite used as filler, which thus opens up a promising scenario for the separation of gaseous mixtures (Boscherini et al., 2021). Indeed, there are recent applications of geopolymers and geopolymer-zeolite composites in carbon capture (Freire et al., 2022), in particular for the separation of CO_2 from flue gases (post-combustion carbon capture) (Zhu et al., 2019), containing mainly nitrogen. Interesting CO_2 capacities have been detected (Pei et al., 2019; Freire et al., 2020; Chen et al., 2021; Candamano et al., 2022; Han et al., 2022), especially in the range of low pressure, but still not quite comparable with those of synthetic zeolites, which represent the benchmark materials for such application (Samanta et al., 2012) and which are obtained following standardized syntheses studied for a long time to maximise the adsorption performances related to their structures.

In this work, a sodium-based commercial zeolite, Na4A ($Na_{12}[(SiO_2)_{12}(AlO_2)_{12}]\cdot 27H_2O$), was selected and incorporated into geopolymer matrices to produce geopolymer-zeolite composites. Such zeolite is characterized by the "Linde Type A" (LTA) structure, which can be described as the union of 8 sodalite cages (β-cages) through 12 cubic secondary building units (SBU) structures (D4R - double four-membered rings). The interconnection gives rise to a central cavity, called α-cage, with a size of about 4 Å, for which zeolite NaA is also called "4A" (Rożek et al., 2019). Zeolite NaA is known for its remarkable CO_2 adsorption capacity (Harper et al., 1969; Indira and Abhitha, 2022), but it is also used in processes of separation by evaporation, as membrane in seawater desalination processes (He et al., 2013). Because of its pronounced hydrophilic character, zeolite NaA can further be used to remove water from organic solutions (Xu et al., 2017) and to control humidity in the air (Takeda et al., 2013). Furthermore, since zeolite NaA, under certain conditions, can spontaneously nucleate from geopolymers (Papa et al., 2018; Rożek et al., 2019), this aspect can be exploited as a more sustainable alternative synthesis compared to the conventional hydrothermal one (Duan et al., 2015). In addition, this *in situ* synthesis from geopolymers allows to control the crystallinity of zeolites, which is not always possible with standard hydrothermal treatments (Alzeer and MacKenzie, 2018). Synthetic zeolites, although more performing than natural zeolites, are obtained by relatively slow, expensive processes that usually use organic templates. Not surprisingly, the research aims to find alternative methods for the synthesis of these materials, including geopolymerization (Duan et al., 2015; Wang et al., 2018; De Rossi et al., 2019; Zheng et al., 2019; Ma et al., 2021; Wu et al., 2021; Ren et al., 2022).

In this study, three metakaolin-based geopolymer matrices were prepared, varying the molar ratio Si:Al and the type of cation (sodium or potassium). A potassium-based matrix with Si:Al = 2 was already proved to have high CO_2 selectivity towards light gases such as nitrogen or methane (Minelli et al., 2016), while the sodium-based matrix with Si:Al = 1.2 allowed the spontaneous nucleation (*in situ* synthesis) of the NaA zeolite during the consolidation process (Papa et al., 2018). Since the presence of NaA crystalline phase is desirable, due to its adsorbing capacity towards CO_2, starting from the geopolymer matrices, composites were prepared adding synthetic zeolite Na4A. Moreover, given the possibility to directly nucleate zeolite NaA starting from the Na-based geopolymer matrix, the latter was added with different amount of synthetic zeolite to verify the total conversion of the matrix into zeolite NaA. The composites were deeply characterized in terms of chemical and microstructural properties and lastly tested for CO_2 adsorption.

2. Materials and methods

2.1. Sample preparations

Metakaolin (grade M1200S, Imerys, SiO_2 = 55%, Al_2O_3 = 39%, SSA = 25 $m^2\ g^{-1}$, D_{50} = 1.5 μm) with an amorphous content of about 87% (Autef et al., 2013) was mixed with NaOH 5 M, KOH 6 M or a potassium silicate solution (K-silicate) with a molar ratio of SiO_2:K_2O = 2.0 and H_2O:K_2O = 13.5 to prepare geopolymer slurries with Si:Al ratio equal 1.2 or 2.0 and coded respectively Na-$G_{1.2}$, K-$G_{1.2}$ and K-G_2, using protocols reported in Papa et al., 2018. Then commercial zeolite Na4A, kindly provided by Luoyang Jianlong Micro-Nano New Materials Co, Ltd. (D_{50} = 3–5 μm, water adsorption ≥27% m/m) and deionized water were added to the geopolymer slurries and mixed with a centrifugal orbital mixer (Thinky Mixer ARE-500, Thinky, Japan) for 3 min at 900 rpm, followed by one minute of defoaming at 1200 rpm.

The composites formulations were firstly set up by a trial-and-error approach to obtain easy-to-cast slurries with the maximum amount of zeolite filler and the minimum quantity of water. Subsequently, the amount of zeolite Na4A, added to the Na-based geopolymer matrix and used also as seed for nucleation, was decreased to assess the possible influence on the conversion of the geopolymer matrix into zeolite NaA.

Table 1
Samples codes, alkaline solution used, Si:Al molar ratio of the consolidated geopolymer matrix, zeolite Na4A wt% and total amount of water (alkaline solution plus added water) used for the slurries preparation.

Sample code	Alkaline solution	Si:Al	Na4A (wt%)	H_2O (wt%)
K-G_2	K-Silicate	2.0	–	30
K-$G_{1.2}$	KOH	1.2	–	44
Na-$G_{1.2}$	NaOH	1.2	–	53
K-G_2-4A	K-Silicate	2.0	22	34
K-$G_{1.2}$-4A	KOH	1.2	25	37
Na-$G_{1.2}$-4A-1	NaOH	1.2	27	45
Na-$G_{1.2}$-4A-2	NaOH	1.2	16	49

Table 1 reports the codes and formulations of the produced geopolymer matrices and composites.

The slurries were cast in cylindrical silicone molds (diameter Ø = 17 mm, height h = 25 mm), then hermetically sealed and placed for 24 h in a heater set at 80 °C. Subsequently, molds were opened and the samples left at 80 °C for further 24 h, to complete the consolidation. 80 °C was the selected temperature to consolidate benchmark geopolymer matrices. This temperature is able to favor and speed up the geopolymerization, obtaining samples with a geopolymerization degree over 97% (Landi et al., 2013), furthermore zeolite A has typically been synthesized at temperature comprised around 60–100 °C (Park et al., 2015). The consolidated materials were then analyzed in bulk or in powder form, after washing at room temperature in distilled water to eliminate the residues of unreacted material.

2.2. Characterization techniques

2.2.1. Chemical and microstructural characterization

Attenuated total reflection (ATR) measurements were performed with a Thermo Scientific Nicolet iS5 FT-IR Spectrometer, with iD7 ATR accessory, to assess the bonds vibrations mode of the samples. The range of acquisition was between 4000 and 400 cm^{-1} and each spectrum was accumulated from 32 individual measurements executed on powder samples.

X-Ray Diffraction (XRD) patterns were obtained using a Powder Diffractometer Bruker D8 Advance with CuKα radiation, Karlsruhe, Germany. The XRD data were analyzed using the RIR method (Chung, 1974), in order to quantify the amount of zeolite NaA. This X-ray diffraction method, applied for quantitative multicomponent analysis, avoid the conventional calibration-curve procedure and a more fundamental 'matrix-flushing' concept is used (Chung, 1974). The matrix-flushing concept gives an exact relationship between intensity and concentration since neither assumption nor approximation is made. Corundum was used as flushing agent and the correct reference intensity for zeolite Na4A was calculated and used to estimate the amount of zeolite NaA presents in the Na-based geopolymer matrix and composites.

The microstructure of the samples was examined by an Environmental Scanning Electron Microscope (*E*-SEM FEI Quanta 200, FEI, Hillsboro, OR, USA). All samples have been covered with a thin layer of gold, to make them conductive, using a turbo-pumped sputter coater (Quorum Q150T ES, Quorum Tech, Laughton, United Kingdom).

Transmission Electron Microscope (TEM) analyses were performed with a FEI TECNAI F20 microscope operating at 200 keV. The powdered samples were suspended in isopropanol and treated in ultrasonic bath for 20 min. The suspension was deposited on a "quantifoil carbon film" Cu grid for TEM analysis and then dried at 100 °C.

The bulk density of the composites was calculated by weight-to-volume ratio, while the true density was obtained analysing the composites powders with a helium pycnometer (Multivolume pycnometer 1305, Micrometrics). Then, total porosity percentage was calculated applying:

$$\text{Total porosity}\% = (1 - (\text{bulk density}/\text{true density}))\ \text{x}100 \quad (1)$$

Mercury Intrusion Porosimetry (MIP) has been used to investigate the pore size distribution of the composites in the range 0.0058–100 μm. The analysis was performed on composites pieces using a Thermo Finningan Pascal 140 and Thermo Finningam Pascal 240, Thermo Fisher Scientific, Waltham, MA, USA.

Specific Surface Area (SSA) values were obtained performing analysis on composites pieces with a Thermo Scientific Surfer instrument (Thermo Fisher Scientific, Waltham, MA, USA), working by nitrogen adsorption at 77 K and applying the Brunauer-Emmett-Teller (BET) method.

2.2.2. CO_2 adsorption tests

The analysis of CO_2 capacity in the geopolymer based composites was performed in a custom-made pressure decay apparatus, using a volumetric method, as already reported in previous publications (Minelli et al., 2016, 2018). Tests were carried out at 35 °C in a differential fashion, with step increases of pressure. The amount of CO_2 adsorbed is evaluated from the pressure decrease of a calibrated volume that contains the sample. Before each test, the sample granules (about 1 g) were conditioned at 200 °C in a vacuum oven, already housed in the holder chamber, and further conditioned at 80 °C under vacuum overnight. The adsorption capacity was calculated from the final chamber pressure at asymptotic time, using the ideal gas law (compressibility factor z is always well near 1 in those conditions). Such procedure was repeated increasing stepwise the pressure up to atmospheric pressure.

3. Results and discussion

3.1. Chemical and microstructural characterization

Since geopolymers and zeolites consist of an aluminosilicate framework, the infrared (IR) region between 1200 and 400 cm^{-1} contains the fundamental vibrations of the framework $(Si,Al)O_4$ (TO_4) tetrahedra and should reflect the framework of the materials (Flanigen et al., 1971). Fig. 1 reports this region of the spectrum for the produced composites and for the commercial zeolite filler Na4A used as reference.

Each zeolite species has a typical infrared pattern and consists of two classes of vibrations: internal vibrations of the framework TO_4-tetrahedron and vibrations due to external linkages between tetrahedra, which are sensitive to the presence of secondary building units, as double rings, and which distinguish the various zeolites. In particular, zeolite A is characterized by the presence of vibrations at ≈ 542 cm^{-1} because of the presence of double rings (D4R). In fact, the presence of this band is evident in all the spectra of the composites reported in Fig. 1. The main peak is located around 950–980 cm^{-1}, because of internal asymmetric stretching vibrations of TO_4 tetrahedra, which are sensitive to framework Si,Al composition since the vibrational frequencies represent the average Si,Al composition and bond characteristics of the central T cation (Flanigen et al., 1971). Regarding the average Si,Al composition it is evident, in Fig. 1a, as this peak is shifted mainly due to the composition of the geopolymer matrix which change from Si:Al = 2.0 to 1.2, with a shift to higher wavenumbers increasing the silica content (Król et al., 2016).

K-based composites showed weaker bands (Fig. 1a), typically for non-crystalline material, associated with the symmetrical stretching (800–600 cm^{-1}) and bending (600–400 cm^{-1}), of the Si-O-Si, Al bonds in the aluminosilicates (Król et al., 2016).

Conversely, the spectra of all Na-based composites are substantially overlapped to that of the starting zeolite Na4A (Fig. 1b). Indeed, in this case the typical zeolite A bands at ≈660 cm^{-1} (TO_4 symmetrical stretching internal vibrations), ≈542 cm^{-1} (double rings vibrations) and ≈460 cm^{-1} (T-O bending), are well evident. This supports the hypothesis that the geopolymer moiety is able to crystallize into NaA crystalline

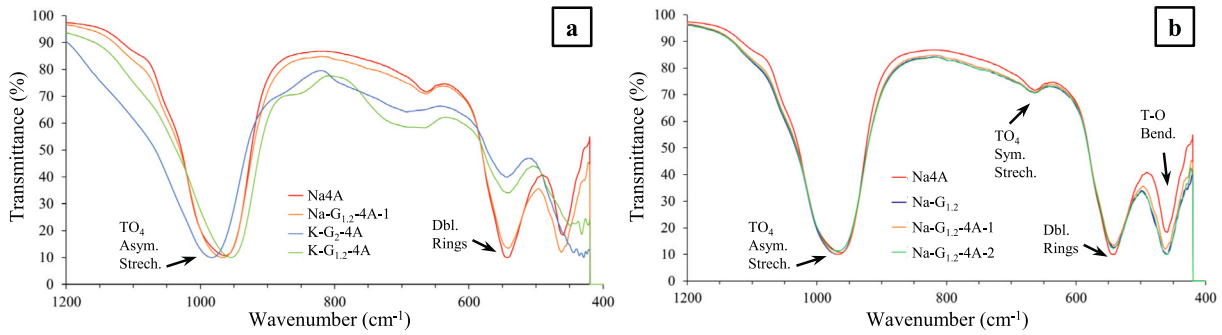

Fig. 1. ATR-FTIR spectra of the zeolite Na4A used as filler and of the synthesized composites Na-$G_{1.2}$-4A-1, K-G_2-4A-1, K-$G_{1.2}$-4A-1 (a). Comparison between the filler Na4A and the Na-based geopolymer matrix and composites (b).

phase during the geopolymerization reaction, in fact, also the spectrum of the Na-$G_{1.2}$ matrix is superimposable with the spectrum of the filler Na4A (Fig. 1b).

In Fig. 2 are reported the XRD spectra of the samples. Regarding the K-based composites (Fig. 2a), in the case of K-G_2-4A, there is the typical hump, centred at 27° of 2θ (Papa et al., 2018), due to the amorphous geopolymer matrix, the peaks related to the crystalline impurities of the starting metakaolin (quartz and muscovite) and the peaks due to the crystalline zeolite Na4A used as filler. K-$G_{1.2}$-4A shows the geopolymer amorphous hump shifted and centred at 30° of 2θ because of the different Si:Al of the matrix. Peaks of crystalline phases, due to impurities of the metakaolin and the zeolite filler, are also evident in this case. In K-based composites ion exchange phenomenon can occur due to the contemporary presence of K cations in the reactive K-based geopolymer slurry and Na cations, present in zeolite Na4A used as filler/seed. K ions do not participate to the nucleation of zeolite A crystals (Warzywoda and Thompson, 1991). When zeolite NaA is used as a seed in K-based synthesis system, some Na ions are exchanged out of the seeds during the synthesis, and nucleation of a new population of zeolite A crystals is not observed (Warzywoda and Thompson, 1991).

Concerning the geopolymer matrix Na-$G_{1.2}$ and the two composites Na-$G_{1.2}$-4A-1 and Na-$G_{1.2}$-4A-2 (Fig. 2b), it is evident as the geopolymer amorphous hump is practically absent and only crystalline phases belonging to zeolite NaA and some impurities of the metakaolin are present. This further confirms how the geopolymer matrix is able to transform itself into zeolite.

Moreover, to evaluate the degree of conversion into zeolite, quantitative analysis has been performed on the Na-based geopolymer matrix and composites, applying the RIR method (Chung, 1974). The method allowed to estimate approximately 81% of zeolite NaA nucleated in the Na-$G_{1.2}$ matrix. The centrifugal orbital mixer, used for the synthesis of these materials, generates a vertical spiral convection in the container allowing an intimate and homogeneous mixing of the reagents, thus favouring the nucleation of NaA in the matrix compared to a mechanical mixing, previously used in Papa et al., 2018, where the formation of NaA was estimated by RIR to be equal to 65%. The addition of different amount of zeolite Na4A, used also as seed for nucleation, did not substantially increased the amount of zeolite NaA, being 82% for both the composites Na-$G_{1.2}$-4A-1 and Na-$G_{1.2}$-4A-2.

In Fig. 3 SEM micrographs of zeolite Na4A, matrix Na-$G_{1.2}$ and of all the synthesized composites are reported, with an evident difference between the sodium and potassium-based materials.

The commercial zeolite filler Na4A (Fig. 3a) is formed by cubic particles, even if some occur with rounded edges and dimensions ranging from about 2 to 5 μm. It is easy to recognize these features also in the Na-based matrix Na-$G_{1.2}$ (Fig. 3b), where it is evident as the cubic zeolite NaA has nucleated starting from the geopolymer matrix. Evidently, the geopolymer matrix has transformed in a significant amount of zeolite NaA, which differs from the commercial one due to the presence of less homogeneous zeolite domains, albeit with a similar size distribution, probably because of a not complete crystallization. Furthermore, the Na-based composites microstructures, showed in Fig. 3 c,d are very similar to the Na-based geopolymer matrix. The typical cubic phases of zeolite NaA are evident in all samples even if with more or less defined edges.

The microstructures of the K-based composites are completely different than cubic zeolite NaA: K-G_2-4A (Fig. 3e) is quite homogeneous resembling the typical geopolymer matrix formed by nanoprecipitates, which embed the zeolite particles of the filler Na4A. Conversely, K-$G_{1.2}$-4A shows a geopolymer matrix poorly cohesive and non-homogeneous, with the presence of flat flakes associable to unreacted metakaolin particles (Fig. 3f). The cubic phases of the zeolite Na4A appear in the geopolymer matrix, but more rounded or in larger aggregates than the commercial one (Fig. 3a).

In Fig. 4 the high resolution TEM images deepen and clarify what was observed with the SEM analyses. In the matrix Na-$G_{1.2}$ the presence of large (2–3 μm) NaA zeolite particles is confirmed (Fig. 4a), and smaller zeolite particles are observed in the early stages of nucleation in the amorphous geopolymer matrix (Fig. 4a,c), as also evident in Na-$G_{1.2}$-4A-1 (Fig. 4c,f).

Conversely, in K-G_2-4A (Fig. 4g,h,i) zeolite 4A particles (2–3 μm) with rounded edge (Fig. 4g) are embedded in agglomerates of nanoparticles (5–50 nm), characteristic of the K-based geopolymer matrix. Finally, composite K-$G_{1.2}$-4A shows the presence of larger agglomerates of geopolymer nanoparticles, as noticed also in the SEM image (Fig. 3f). Probably, in this last case, the highly alkaline geopolymerization conditions have affected the zeolite filler modifying it superficially, rounding the vertices and edges of the cubic structure. This likely due to the nucleation of an additional K-substituted zeolite fraction resulting in formation of larger aggregates.

3.2. *Porosity characterization of the composites*

Table 2 shows the data of bulk and true density, total porosity %, the main values obtained by Mercury Intrusion Porosimetry (MIP) analysis and the specific surface area (SSA) values of the three most representative composites.

The bulk density is inclusive of both the solid material and the total porosity (closed and open). Conversely, true density does not consider the porosity and depends on the stoichiometry, indeed it increases increasing the Si:Al ratio, since silicon has a greater atomic mass than aluminum. Furthermore, true density depends on the type of cation, and in general, with the same charge, it increases as its atomic mass increases, as in the case of the potassium-based composite compared to the sodium-based one.

The open porosity and the specific surface area also depend on the composition of the material and, in particular, as the Si:Al ratio increases, there is an increase in the surface area and a decrease in porosity detected by MIP, due to the change in the average size of the pores (Papa et al., 2018). All the trends described can be observed in the values

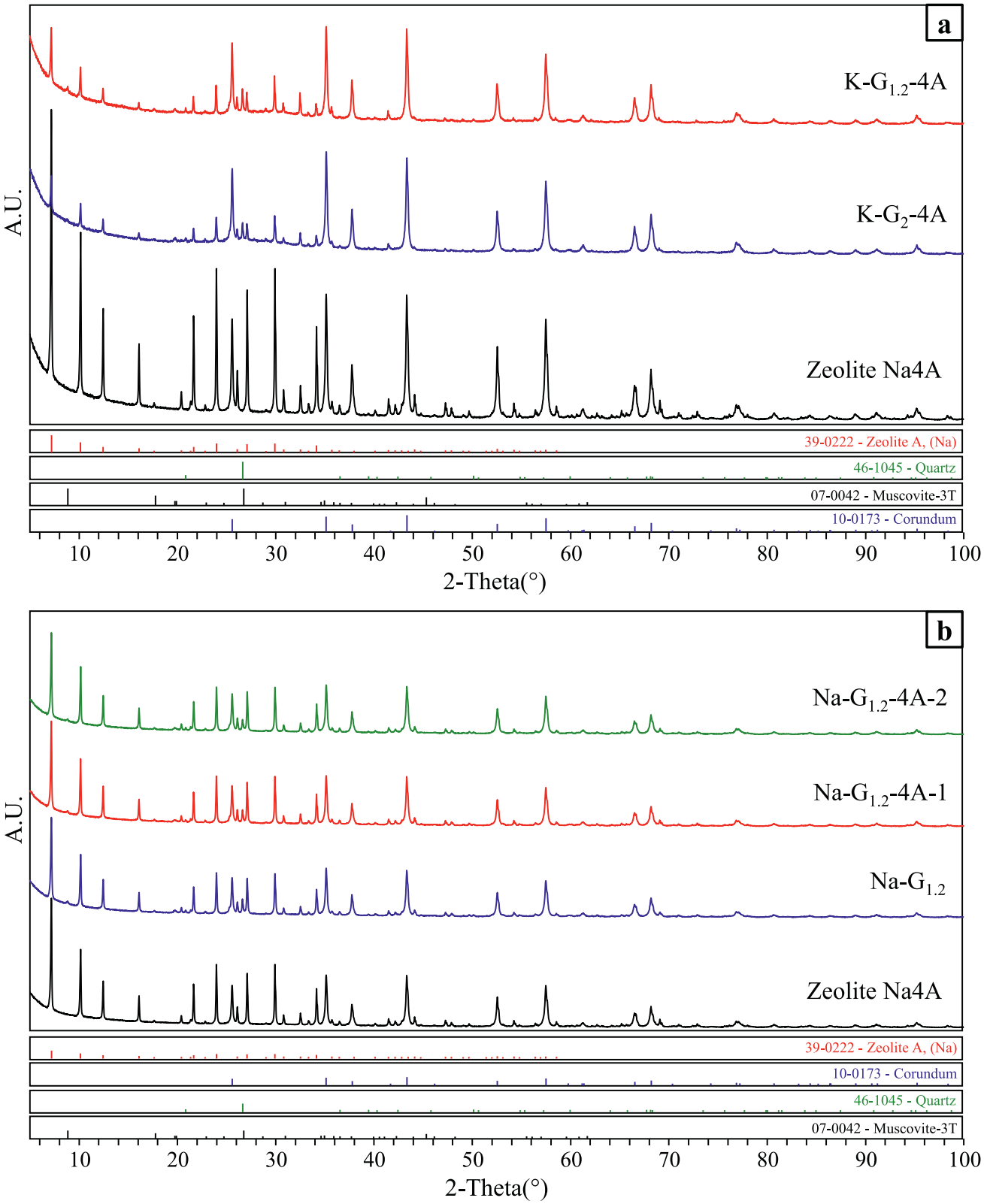

Fig. 2. XRD diffractograms of synthesized composites K-G_2-4A-1, K-$G_{1.2}$-4A-1, Na-$G_{1.2}$-4A-1, compared with the commercial zeolite Na4A used as filler. Samples were mixed with corundum, to perform an estimation of the different phases by RIR method.

reported in Table 2 for the synthesized composites.

The pore size distributions, obtained by MIP, are reported in Fig. 5. MIP analysis provides a good interpretation of the distribution of the meso- and macro-pores, in the range 0.0058–100 μm, therefore mainly due to the geopolymer matrix, since it is not able to detect the zeolite micro-porosity, while other methods are used (Mańko et al., 2013). In general, all distributions are monomodal but with different modal pore diameter (most frequent pore size) (Table 2), being 0.06 μm for K-G_2-4A,

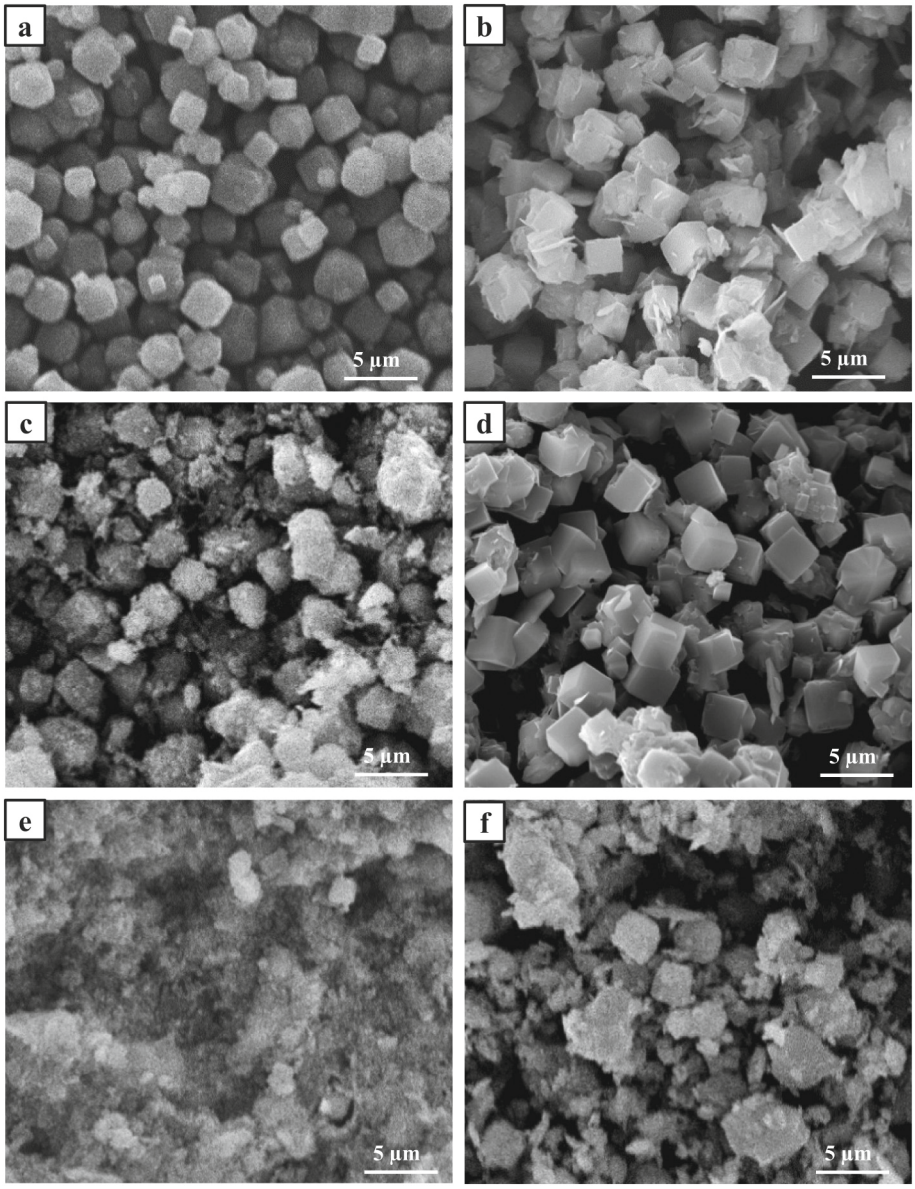

Fig. 3. SEM micrographs of a) zeolite filler Na4A, b) Na-$G_{1.2}$ matrix, c) Na-$G_{1.2}$-4A-1, d) Na-$G_{1.2}$-4A-2, e) K-G_2-4A and f) K-$G_{1.2}$-4A composites.

0.63 µm for K-$G_{1.2}$-4A and 1.84 µm for Na-$G_{1.2}$-4A-1. As reported previously, porosity depends on the geopolymer composition: the larger Si:Al ratio, the lower the pores diameter with a higher frequency. It follows that in the case of K-G_2-4A, although the modal pore is just "outside" the mesoporosity range (2–50 nm), the most part of the pore size distribution is "inside" because of the presence of a tight geopolymer matrix acting as a binder for zeolite NaA. In the case of K-$G_{1.2}$-4A, the modal pore diameter is shifted at higher value both for the lower Si:Al ratio and for the formation of agglomerates which increase the porosity in the composite, as visible in Fig. 3f. Finally, in Na-$G_{1.2}$-4A-1, the value of the modal pore size can be associated with the pores present between the various zeolite particles (both added and *in situ* formed), as evident from the SEM image (Fig. 3c). It is important to mention that as MIP technique is not able to evaluate the micro-porosity of the zeolite, even BET surface area analysis is not able to determine the contribution provided by the zeolite to the overall surface area, as the limit dimension for N_2 to penetrate inside the pores at 77 K is 5 Å (García-Martínez et al., 2000), while the NaA zeolite has a size of 4 Å.

3.3. CO_2 adsorption capacity

Figure 6 shows the adsorption isotherms, obtained by averaging at least three replicates of the analysis. The Dual Site Langmuir (DSL) model (Minelli et al., 2018) was used to describe the experimental data. In detail, the adsorbing capacities against carbon dioxide at the reference temperature 35 °C and measured in a sub-atmospheric pressure range from 0 to 1 atm are reported.

In K-based composites, the addition of zeolite Na4A does not lead to an increase in CO_2 adsorption capacity, as previously found thanks to the addition of commercial zeolite Na13X (with faujasite-type structure an effective pore size of 10 Å) in composite K-G_2-Z2 (Papa et al., 2018; Minelli et al., 2018) (Table 3). As one can see, K-$G_{1.2}$-4A shows basically no CO_2 capacity throughout the pressure range investigated, while K-G_2-4A shows almost the same CO_2 adsorption curve than that of the K-based geopolymer matrix (Minelli et al., 2018). However, as mentioned before, ion exchange phenomena probably occurred during the reaction synthesis because of the contemporary presence of a reactive K-based geopolymer slurry and Na-based zeolite 4A. The different behaviour of these composites compared to those made with the addition of Na13X

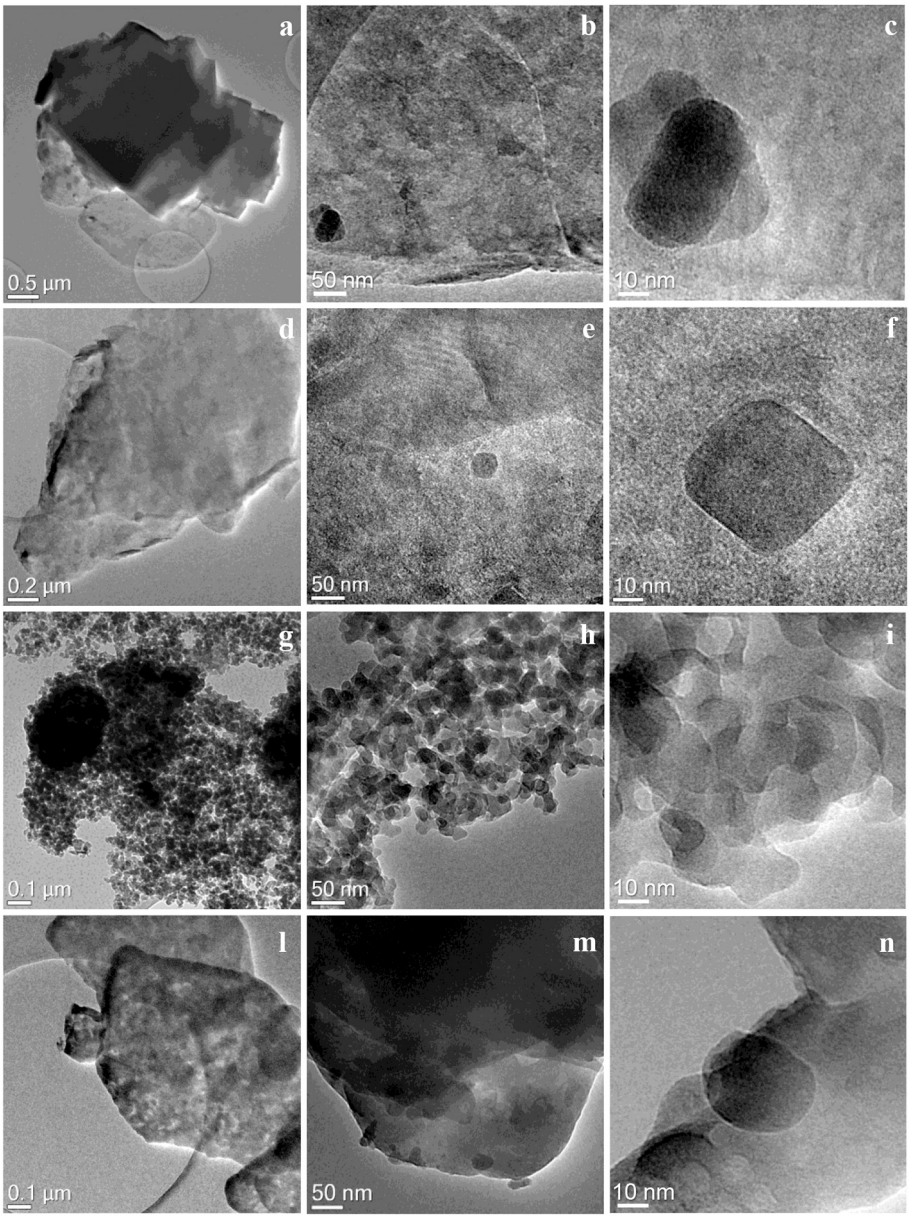

Fig. 4. TEM images of Na-$G_{1.2}$ geopolymer matrix (a,b,c) and of the composites Na-$G_{1.2}$-4A-1 (d,e,f), K-G_2-4A (g,h,i) and K-$G_{1.2}$-4A (l,m,n).

Table 2
Bulk and true density and calculated total porosity %. The main values obtained by MIP: open porosity, total pore volume, average and modal pore diameters. Specific surface area (SSA) values of the composites.

Sample code	Bulk D ($g\ cm^{-3}$)	True D ($g\ cm^{-3}$)	Total Porosity (%)	Open Porosity (%)	Tot pore volume ($mm^3\ g^{-1}$)	Average pore Ø (µm)	Modal pore Ø (µm)	SSA ($m^2\ g^{-1}$)
K-G_2-4A	1.02 ± 0.02	2.18 ± 0.01	53	49	440	0.04	0.06	37
K-$G_{1.2}$-4A	0.98 ± 0.01	2.15 ± 0.01	55	55	562	0.18	0.63	8
Na-$G_{1.2}$-4A-1	0.88 ± 0.01	2.04 ± 0.01	57	51	569	0.32	1.84	11

(in which the adsorption capacity was the sum of the relative contributions of zeolite Na13X and K-based geopolymer matrix, Minelli et al., 2018) is likely related to the higher cation exchange capacity of zeolite Na4A with respect to zeolite Na13X, due to the different structures and free openings of the channels (size windows) (García-Sosa and Solache-Ríos, 2001). The larger dimension of potassium than sodium, having a smaller charge concentration, leads to a reduced or null electrostatic interaction with CO_2 in the K-exchanged A zeolite.

Different results were obtained for the Na-$G_{1.2}$-4A-1 composite, which showed a relatively high adsorbing capacity (Table 3). The main difference depends on the presence of sodium as a cation in the reactive geopolymer slurry, which on the one hand leads to a faster and more complete hydrolysis of the reactive powder than potassium and on the other allows the nucleation of a further fraction of zeolite NaA with respect to the added one. The high charge of sodium implies a great electrostatic interaction with CO_2.

The obtained CO_2 capacities are in any case larger at lower pressure values (corresponding to the typical CO_2 partial pressure in post

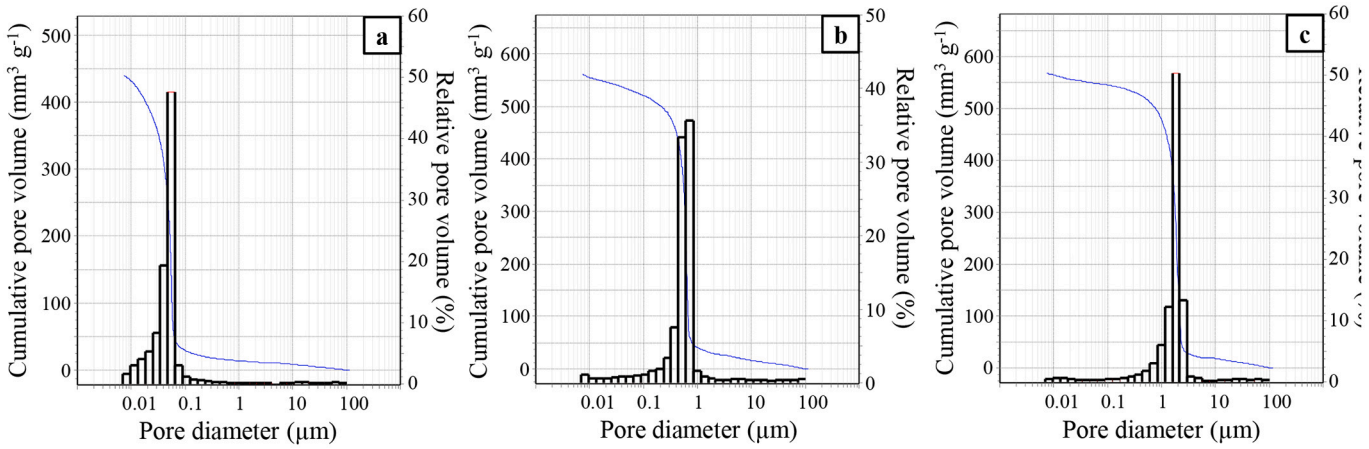

Fig. 5. Pore size distributions by MIP of composites a) K-G_2-4A, b) K-$G_{1.2}$-4A and c) Na-$G_{1.2}$-4A-1.

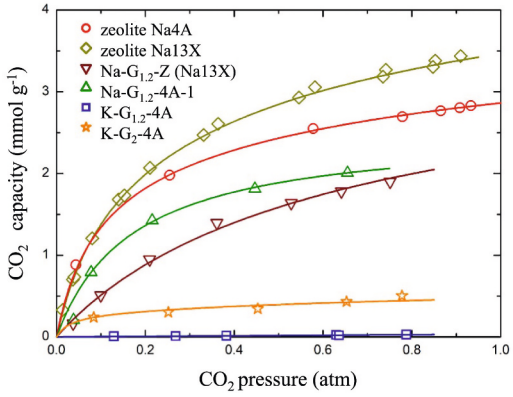

Fig. 6. CO_2 adsorption capacity in neat zeolite Na4A and in the geopolymer-zeolite composites at 35 °C. The samples were compared with neat zeolite Na13X and composite Na-$G_{1.2}$-Z (Na13X) reported in Minelli et al., 2018. Lines are obtained using a Dual Site Langmuir correlation.

Table 3
Values of CO_2 adsorption capacity at 0.1 bar and 1 bar, calculated according to Dual Site Langmuir (DSL) model (Minelli et al., 2018).

Adsorbent	CO_2 capacity qCO_2 (mmol g^{-1})		Reference
	0.1 bar	1 bar	
K-G_2-4A	0.25	0.47	This work
K-$G_{1.2}$-4A	0.003	0.03	This work
Na-$G_{1.2}$-4A	1.0	2.6	This work
Na4A	1.2	2.9	This work
Na13X	1.4	3.5	Minelli et al., 2018
K-G_2-Z2 (Na13X)	0.75	1.6	Minelli et al., 2018
Na-$G_{1.2}$-Z (Na13X)	1.1	2.5	Minelli et al., 2018

combustion carbon capture application) than those of the Na-$G_{1.2}$-Z (Na13X) composite (Minelli et al., 2018) (Table 3), while at higher pressure the CO_2 capacity is similar as in in the case of zeolite Na4A and Na13X (Minelli et al., 2018). Nevertheless, the adsorption value of the Na-$G_{1.2}$-4A-1 composite is comparable with that of the commercial zeolite NaA in powder form (and close to pure zeolite Na13X, the current benchmark material for carbon capture application), but with the advantage of the simple shaping of the material. In fact, since on an industrial level it is necessary to resort to the use of binders to support and form the zeolites, the performance of the zeolites is significantly reduced. This drawback can be avoided by using a geopolymer support, which would allow the obtainment of a carrier material without decreasing the adsorbing properties characterizing the zeolites.

4. Conclusion

Starting from three metakaolin-based geopolymer matrices, varying in Si:Al molar ratio (2.0 or 1.2) and type of cation (sodium or potassium), geopolymer-zeolite composites were synthesized adding a commercial synthetic zeolite Na4A in order to produce post combustion CO_2 adsorbents.

In general, the geopolymer matrices act as binders allowing the shaping of zeolite and determining the different chemical composition, microstructure and porosity of the final composites.

The sodium-based geopolymer matrix with Si:Al = 1.2 (Na-$G_{1.2}$) allowed the spontaneous *in situ* nucleation of the zeolite NaA, approximately estimated to be 81%. Two different amounts of synthetic zeolite Na4A were added as seed for nucleation to matrix. However, the addition of syntethic zeolite did not substantially increased the amount of zeolite NaA, being 82% for both composites (Na-$G_{1.2}$-4A-1 and Na-$G_{1.2}$-4A-2).

Regarding the CO_2 adsorption capacity, the K-based composites (K-G_2-4A and K-$G_{1.2}$-4A) exhibited low values because the beneficial effect given by the presence of zeolite Na4A was cancelled by ion exchange phenomena that occurred during the reaction synthesis due to the contemporary presence of a reactive K-based geopolymer slurry and Na-based zeolite 4A.

Conversely the Na-based composite (Na-$G_{1.2}$-4A-1) was the best performing with an adsorption capacity of 1.0 mmol g^{-1} at 0.1 bar and 2.6 mmol g^{-1} at 1 bar, nearly equivalent to synthetic zeolite Na4A and close to pure zeolite Na13X, the current benchmark material for carbon capture application.

CRediT authorship contribution statement

Elettra Papa: Writing – original draft, Investigation, Conceptualization, Visualization. **Matteo Minelli:** Conceptualization, Methodology, Investigation. **Maria Chiara Marchioni:** Investigation. **Elena Landi:** Conceptualization. **Francesco Miccio:** Conceptualization. **Annalisa Natali Murri:** Writing – review & editing. **Patricia Benito:** Supervision. **Angelo Vaccari:** Supervision. **Valentina Medri:** Writing – original draft, Conceptualization, Supervision, Writing – review & editing.

Declaration of Competing Interest

The authors declare that they have no known competing financial interests or personal relationships that could have appeared to influence the work reported in this paper.

Data availability

Data will be made available on request.

Acknowledgments

Project funded under the National Recovery and Resilience Plan (NRRP), Mission 04 Component 2 Investment 1.5 – NextGenerationEU, Call for tender n. 3277 dated 30/12/2021 Award Number: 0001052 dated 23/06/2022. The authors greatly thank Luoyang Jianlong Micro-Nano New Materials Co, Ltd. that kindly provided zeolite Na4A, Mattia Boscherini for CO_2 adsorption tests and Dr. Francesca Ospitali for TEM analyses.

References

Alzeer, M.I.M., MacKenzie, K.J.D., 2018. Synthesis and catalytic properties of new sustainable aluminosilicate heterogeneous catalysts derived from fly ash. ACS Sustain. Chem. Eng. 6 (4), 5273–5282. https://doi.org/10.1021/acssuschemeng.7b04923.

Autef, A., Joussein, E., Poulesquen, A., Gasgnier, G., Pronier, S., Sobrados, I., Sanz, J., Rossignol, S., 2013. Influence of metakaolin purities on potassium geopolymer formulation: the existence of several networks. J. Colloid Interface Sci. 408, 43–53. https://doi.org/10.1016/j.jcis.2013.07.024.

Boscherini, M., Miccio, F., Papa, E., Medri, V., Landi, E., Doghieri, F., Minelli, M., 2021. The relevance of thermal effects during CO_2 adsorption and regeneration in a geopolymer-zeolite composite: Experimental and modelling insights. Chem. Eng. J. 408, 127315 https://doi.org/10.1016/j.cej.2020.127315.

Breck, D.W., 1974. Zeolite Molecular Sieves: Structure, Chemistry, and Use. John Wiley and Sons Inc., New York.

Candamano, S., Policicchio, A., Conte, G., Abarca, R., Algieri, C., Chakraborty, S., Curcio, S., Calabrò, V., Crea, F., Agostino, R.G., 2022. Preparation of foamed and unfoamed geopolymer/NaX zeolite/activated carbon composites for CO_2 adsorption. J. Clean. Prod. 330, 129843 https://doi.org/10.1016/j.jclepro.2021.129843.

Chen, H., Zhang, Y.J., He, P.Y., Liu, L.C., 2021. Synthesis, characterization, and selective CO_2 capture performance of a new type of activated carbon-geopolymer composite adsorbent. J. Clean. Prod. 325, 129271 https://doi.org/10.1016/j.jclepro.2021.129271.

Chung, F.H., 1974. Quantitative interpretation of X-ray diffraction patterns of mixtures. I. matrix-flushing method for quantitative multicomponent analysis. J. Appl. Crystallogr. 7, 519–525.

Cong, P., Cheng, Y., 2021. Advances in geopolymer materials: a comprehensive review. J. Traffic Transp. Eng. 8 (3), 283–314. https://doi.org/10.1016/j.jtte.2021.03.004.

Davidovits, J., 1991. Geopolymers, Inorganic polymeric new materials. J. Therm. Anal. 37, 1633–1656. https://doi.org/10.1007/BF01912193.

Davidovits, J., 2008. Geopolymer Chemistry and Applications. Geopolymer Institute, Saint-Quentin. ISBN 2951482019, 9782951482012.

De Rossi, A., Simão, L., Ribeiro, M.J., Novais, R.M., Labrincha, J.A., Hotza, D., Moreira, R.F.P.M., 2019. In-situ synthesis of zeolites by geopolymerization of biomass fly ash and metakaolin. Mater. Lett. 236, 644–648. https://doi.org/10.1016/j.matlet.2018.11.016.

Duan, J., Li, J., Lu, Z., 2015. One-step facile synthesis of bulk zeolite a through metakaolin-based geopolymer gels. J. Porous. Mater. 22 (6), 1519–1526. https://doi.org/10.1007/s10934-015-0034-6.

Duxson, P., Provis, J.L., Lukey, G.C., Mallicoat, S.W., Kriven, W.M., Van Deventer, J.S.J., 2005. Understanding the relationship between geopolymer composition, microstructure and mechanical properties. Colloids Surf. A Physicochem. Eng. Asp. 269, 47–58. https://doi.org/10.1016/j.colsurfa.2005.06.060.

Flanigen, E.M., Khatami, H., Szymanski, H.A., 1971. Infrared Structural Studies of Zeolite Frameworks. In: Flanigen, E.M., Sand, L.B. (Eds.), Molecular Sieve Zeolites, Advances in Chemistry, vol. 101. American Chemical Society, Washington DC, pp. 201–229. https://doi.org/10.1021/ba-1971-0102.

Freire, A.L., Moura-Nickel, C.D., Scaratti, G., De Rossi, A., Araújo, M.H., Agenor, D.N.J., Rodrigues, A.E., Castellón, E.R., Moreira, R.D.F.P.M., 2020. Geopolymers produced with fly ash and rice husk ash applied to CO_2 capture. J. Clean. Prod. 273, 122917 https://doi.org/10.1016/j.jclepro.2020.122917.

Freire, A.L., José, H.J., Moreira, R.D.F.P.M., 2022. Potential applications for geopolymers in carbon capture and storage. Int. J. Greenh. Gas Control 118, 103687. https://doi.org/10.1016/j.ijggc.2022.103687.

García-Martínez, J., Cazorla-Amorós, D., Linares-Solano, Á., 2000. Further evidences of the usefulness of CO_2 adsorption to characterize microporous solids. Stud. Surf. Sci. Catal. 128, 485–494. https://doi.org/10.1016/S0167-2991(00)80054-3.

García-Sosa, I., Solache-Ríos, M., 2001. Cation-exchange capacities of zeolites A, X, Y, ZSM-5 and Mexican erionite compared with the retention of cobalt and cadmium. J. Radioanal. Nucl. Chem. 250, 205–206.

Han, L., Wang, X., Wu, B., Zhu, S., Wang, J., Zhang, Y., 2022. In-situ synthesis of zeolite X in foam geopolymer as a CO_2 adsorbent. J. Clean. Prod. 372, 133591 https://doi.org/10.1016/j.jclepro.2022.133591.

Harper, R.J., Stifel, G.R., Anderson, R.B., 1969. Adsorption of gases on 4A synthetic zeolite. Can. J. Chem. 47 (24), 4661–4670. https://doi.org/10.1139/v69-770.

He, Y., Cui, X., Liu, X., Wang, Y., Zhang, J., Liu, K., 2013. Preparation of self-supporting NaA zeolite membranes using geopolymers. J. Membr. Sci. 447, 66–72. https://doi.org/10.1016/j.memsci.2013.07.027.

Huang, Y., Han, M., Yi, R., 2012. Microstructure and properties of fly ash-based geopolymeric material with 5A zeolite as a filler. Constr. Build. Mater. 33, 84–89. https://doi.org/10.1016/j.conbuildmat.2012.01.014.

Indira, V., Abhitha, K., 2022. A review on recent developments in Zeolite A synthesis for improved carbon dioxide capture: implications for the water-energy nexus. Energy Nexus 7, 100095. https://doi.org/10.1016/j.nexus.2022.100095.

Khaleque, A., Alam, M.M., Hoque, M., Mondal, S., Haider, J.B., Xu, B., Johir, M.A.H., Karmakar, A.K., Zhou, J.L., Ahmed, M.B., Moni, M.A., 2020. Zeolite synthesis from low-cost materials and environmental applications: a review. Environ. Adv. 2, 100019 https://doi.org/10.1016/j.envadv.2020.100019.

Kriven, W.M., Bell, J.L., Gordon, M., 2003. Microstructure and microchemistry of fully-reacted geopolymers and geopolymer matrix composites. Ceram. Trans. 153, 227–250.

Król, M., Minkiewicz, J., Mozgawa, W., 2016. IR spectroscopy studies of zeolites in geopolymeric materials derived from kaolinite. J. Mol. Struct. 1126, 200–206. https://doi.org/10.1016/j.molstruc.2016.02.027.

Landi, E., Medri, V., Papa, E., Dedecek, J., Klein, P., Benito, P., Vaccari, A., 2013. Alkali-bonded ceramics with hierarchical tailored porosity. Appl. Clay Sci. 73, 56–64. https://doi.org/10.1016/j.clay.2012.09.027.

Lee, N., Khalid, H., Lee, H.K., 2016. Synthesis of mesoporous geopolymers containing zeolite phases by a hydrothermal treatment. Microporous Mesoporous Mater. 229, 22–30. https://doi.org/10.1016/j.micromeso.2016.04.016.

Liu, Y., Yan, C., Qiu, X., Li, D., Wang, H., Alshameri, A., 2016. Preparation of faujasite block from fly ash-based geopolymer via in-situ hydrothermal method. J. Taiwan Inst. Chem. Eng. 59, 433–439. https://doi.org/10.1016/j.jtice.2015.07.012.

Ma, G., Bai, C., Wang, M., He, P., 2021. Effects of Si/Al ratios on the bulk-type zeolite formation using synthetic metakaolin-based geopolymer with designated composition. Crystals 11, 1310. https://doi.org/10.3390/cryst11111310.

Mańko, M., Chal, R., Trens, P., Minoux, D., Gérardin, C., Makowski, W., 2013. Porosity of micro–mesoporous zeolites prepared via pseudomorphic transformation of zeolite Y crystals: a combined isothermal sorption and thermodesorption investigation. Microporous Mesoporous Mater. 170, 243–250. https://doi.org/10.1016/j.micromeso.2012.12.016.

Medri, V., Fabbri, S., Dedecek, J., Sobalik, Z., Tvaruzkova, Z., Vaccari, A., 2010. Role of the morphology and the dehydroxylation of metakaolins on geopolymerization. Appl. Clay Sci. 50, 538–545. https://doi.org/10.1016/j.clay.2010.10.010.

Minelli, M., Medri, V., Papa, E., Miccio, F., Landi, E., Doghieri, F., 2016. Geopolymers as solid adsorbent for CO_2 capture. Chem. Eng. Sci. 148, 267–274. https://doi.org/10.1016/j.ces.2016.04.013.

Minelli, M., Papa, E., Medri, V., Miccio, F., Benito, P., Doghieri, F., Landi, E., 2018. Characterization of novel geopolymer – Zeolite composites as solid adsorbents for CO_2 capture. Chem. Eng. J. 341, 505–515. https://doi.org/10.1016/j.cej.2018.02.050.

Papa, E., Medri, V., Amari, S., Manaud, J., Benito, P., Vaccari, A., Landi, E., 2018. Zeolite-geopolymer composite materials: production and characterization. J. Clean. Prod. 171, 76–84. https://doi.org/10.1016/j.jclepro.2017.09.270.

Park, S.H, Yang, J.K., Kim, J.H, Chung, C.B., Seo, G., 2015. Eco-friendly synthesis of zeolite A from synthesis cakes prepared by removing the liquid phase of aged synthesis mixtures. Green Chem 17, 3571–3578. https://doi.org/10.1039/C5GC00854A.

Pei, Y.-R., Choi, G., Asahina, S., Yang, J.-H., Vinu, A., Choy, J.-H., 2019. A novel geopolymer route to porous carbon: high CO_2 adsorption capacity. Chem. Commun. 55, 3266–3269. https://doi.org/10.1039/C9CC00232D.

Ren, B., Zhao, Y., Bai, H., Kang, S., Zhang, T., Song, S., 2021. Eco-friendly geopolymer prepared from solid wastes: a critical review. Chemosphere 267, 128900. https://doi.org/10.1016/j.chemosphere.2020.128900.

Ren, Z., Wang, L., Li, Y., Zha, J., Tian, G., Wang, F., Zhang, H., Liang, J., 2022. Synthesis of zeolites by in-situ conversion of geopolymers and their performance of heavy metal ion removal in wastewater: a review. J. Clean. Prod. 349, 131441 https://doi.org/10.1016/j.jclepro.2022.131441.

Romero, P., Nishant, G., 2022. Evolution of kaolinite morphology upon exfoliation and dissolution: evidence for nanoscale layer thinning in metakaolin. Appl. Clay Sci. 222, 106486 https://doi.org/10.1016/j.clay.2022.106486.

Rożek, P., Król, M., Mozgawa, W., 2019. Geopolymer-zeolite composites: a review. J. Clean. Prod. 230, 557–579. https://doi.org/10.1016/j.jclepro.2019.05.152.

Samanta, A., Zhao, A., Shimizu, G.K.H., Sarkar, P., Gupta, R., 2012. Post-Combustion CO_2 capture using solid Sorbents: a review. Ind. Eng. Chem. Res. 51, 1438–1463. https://doi.org/10.1021/ie200686q.

Takeda, H., Hashimoto, S., Yokoyama, H., Honda, S., Iwamoto, Y., 2013. Characterization of Zeolite in Zeolite-Geopolymer hybrid bulk materials derived from kaolinitic clays. Mater. 6 (5), 1767–1778. https://doi.org/10.3390/ma6051767.

Wang, H., Yan, C., Li, D., Zhou, F., Liu, Y., Zhou, C., Komarneni, S., 2018. In situ transformation of geopolymer gels to self-supporting NaX zeolite monoliths with excellent compressive strength. Microporous Mesoporous Mater. 261, 164–169. https://doi.org/10.1016/j.micromeso.2017.11.015.

Warzywoda, J., Thompson, R.W., 1991. Synthesis of zeolite A in the Na/K system and the effect of seeding. Zeolites 11 (6), 577–582. https://doi.org/10.1016/S0144-2449(05)80008-9.

Wu, D., Huang, Y., Xiao, G., Li, X., Yao, X., Deng, Z., Tan, R., 2021. In situ synthesis of zeolites by geopolymerization with NaOH/KOH mixed solution and their potential application for Cd(II) immobilization in paddy soil. Clay Miner. 56 (2), 156–167. https://doi.org/10.1180/clm.2021.29.

Wu, Z., Liu, H., Chen, T., Cheng, P., Wang, C., Kong, D., 2018. Preparation, characterization, and performance of 4A zeolite based on opal waste rock for removal of ammonium ion. Adsorpt. Sci. Technol. 36 (9–10), 1700–1715. https://doi.org/10.1177/0263617418803012.

Xu, M., He, Y., Wang, Y., Cui, X., 2017. Preparation of a non-hydrothermal NaA zeolite membrane and defect elimination by vacuum-inhalation repair method. Chem. Eng. Sci. 158, 117–123. https://doi.org/10.1016/j.ces.2016.10.001.

Zhang, X., Bai, C., Qiao, Y., Wang, X., Jia, D., Li, H., Colombo, P., 2021. Porous geopolymer composites: a review. Compos. Part A Appl. Sci. Manuf. 150, 106629 https://doi.org/10.1016/j.compositesa.2021.106629.

Zheng, Z., Ma, X., Zhang, Z., Li, Y., 2019. In-situ transition of amorphous gels to Na-P1 zeolite in geopolymer: mechanical and adsorption properties. Constr. Build. Mater. 202, 851–860. https://doi.org/10.1016/j.conbuildmat.2019.01.067.

Zhu, X., Li, S., Shi, Y., Cai, N., 2019. Recent advances in elevated-temperature pressure swing adsorption for carbon capture and hydrogen production. Prog. Energy Combust. Sci. 75, 100784 https://doi.org/10.1016/j.pecs.2019.100784.